arXiv:1609.03997v1 [astro-ph.CO] 13 Sep 2016

Calibrating Cluster Number Counts with CMB lensing

Thibaut Louis[1] and David Alonso[2]
[1] *UPMC Univ Paris 06, UMR7095, Institut d'Astrophysique de Paris, F-75014, Paris, France*
[2] *University of Oxford, Denys Wilkinson Building, Keble Road, Oxford OX1 3RH, UK*
(Dated: September 14, 2016)

CMB Stage-4 experiments will reduce the uncertainties on the gravitational lensing potential by an order of magnitude compared to current measurements, and will also produce a Sunyaev-Zel'dovich (SZ) cluster catalog containing $\sim 10^5$ objects, two orders of magnitudes higher than what is currently available. In this paper we propose to combine these two observables and show that it is possible to calibrate the masses of the full Stage-4 cluster catalog internally owing to the high signal to noise measurement of the CMB lensing convergence field. We find that a CMB Stage-4 experiment will constrain the hydrostatic bias parameter to sub-percent accuracy. We also show constraints on a non parametric $Y-M$ relationship which could be used to study its evolution with mass and redshift. Finally we present a joint likelihood for thermal SZ (tSZ) flux and mass measurements, and show that it could lead to a $\sim 5\sigma$ detection of the lower limit on the sum of the neutrino masses in the normal hierarchy ($\sum m_\nu = 60$meV) once combined with measurements of the primordial CMB and CMB lensing power spectra.

I. INTRODUCTION

The number of galaxy clusters as a function of mass and redshift is a prediction of the LCDM model, and by accurately reconstructing the cluster mass function we can put constraints on cosmological parameters such as the matter density Ω_m, the sum on the neutrinos masses $\sum m_\nu$ and the normalisation of the linear matter power spectrum σ_8. This observable has recently gained a vivid interest following the publication of the Planck cluster catalog ($\approx 10^3$ clusters) and the slight discrepancy between cosmological parameters inferred from the primary CMB and from the distribution of cluster masses [1, 2].

A classical method to estimate cluster masses is to use measurements of the Compton-y parameter, a measurement of the integrated flux of the thermal Sunyaev-Zel'dovich effect at the position of the cluster. The size of the effect is proportional to the total thermal energy of the cluster gas and is therefore correlated with cluster mass [3–5]. This $Y-M$ scaling relation has traditionally been determined empirically from X-ray observations of clusters [6, 7]. However, X-ray-inferred cluster masses rely on the assumption that clusters have reached hydrostatic equilibrium, and departure from this equilibrium can bias the estimated cluster masses. Physical phenomena causing this departure include bulk motions in the gas or non-thermal sources of pressure (such as magnetic fields or cosmic rays). Numerical simulations have shown that this can lead to an underestimation of the true cluster masses by 10 to 15 % [8–10]. Moreover, instrumental systematics in the X-ray analysis could propagate into the cosmological results [11], and an independent method for calibrating the scaling relation is extremely valuable.

Following the first detections of CMB lensing by clusters [12, 13], a new method for self-calibrating the cluster masses using measurements of the lensing convergence at the cluster positions has recently been proposed [14]. It has been demonstrated on simulations and successfully applied to Planck data resulting in a 5σ measurement of the hydrostatic bias parameter [2]. The aim of this work is to discuss extensions of this method in the era of CMB Stage-4 (S4), a next-generation CMB experiment that will achieve a cosmic-variance-limited reconstruction of the convergence field up to multipoles $\ell \sim 1000$.

This paper is structured as follows. In Section II we describe our cluster lensing model as well as a maximum likelihood estimator for the cluster masses from a lensing convergence map. We also discuss the impact of possible foregrounds contamination and atmospheric noise. In Section III we propose two parametric methods to calibrate the $Y-M$ relationship using cluster lensing. First we forecast constraints on the hydrostatic parameter following the method proposed in [14], and then extend the formalism and forecast constraints on more general scaling relations, including a non-parametric model that can be used to study the mass and redshift dependence freely. In Section IV we study how the availability of joint tSZ and lensing mass measurements improves the cosmological constraints achievable by a cluster survey carried out with S4 by consistently accounting for the uncertainties in the $Y-M$ scaling relation. We summarise our main conclusions in Section V.

Throughout this paper we adopt a fiducial cosmology with $\Omega_m = 0.315$, $\Omega_b = 0.049$, $\Omega_\Lambda = 0.685$, $H_0 = 67\,\mathrm{km\,s^{-1}Mpc^{-1}}$, $A_s = 2.2\times10^{-9}$, $n_s = 0.96$ and $\tau = 0.06$, compatible with [15]. We will use cluster masses M_{500} defined as the mass measured within a radius R_{500} that encloses a mean density 500 times larger than the critical density at the cluster redshift. We will also estimate the number density of haloes as a function of mass using the measurements of the mass function by [16].

II. CLUSTER LENSING MODEL

The potential of CMB lensing to determine cluster masses has been long recognised [17–20]. In this sec-

tion, we follow [14] and describe a maximum likelihood estimator for clusters masses based on measurements of the lensing convergence map. We then discuss the noise properties of CMB Stage-4, and the possible contamination of the lensing field reconstructed from temperature data due to atmospheric noise and foregrounds.

A. Matched filter estimate of cluster masses

We start by modelling the cluster mass distribution using a NFW profile [21]

$$\rho(x) = \frac{\rho_0}{(c_{500}x_r)(1+(c_{500}x_r))^2} \tag{1}$$

where ρ_0 is the central mass density, x is a dimensionless radial variable $x_r = r/R_{500}$ and c_{500} is the concentration parameter. In what follows we will use a constant concentration $c_{500} = 1.18$. The halo lensing convergence can be related to the cluster surface mass density via $\kappa(\boldsymbol{x}) = \Sigma(\boldsymbol{x})/\Sigma_{\rm crit}$, where

$$\Sigma(\boldsymbol{x}) \equiv \int_{-\infty}^{\infty} dl\, \rho(l,\boldsymbol{x}),\ \ \Sigma_{\rm crit} \equiv \frac{c^2 d_S}{4\pi G\, d_L\, d_{LS}}. \tag{2}$$

Here d_L, d_S, and d_{LS} are the angular diameter distances to the lens (the cluster), the source (the CMB) and the angular diameter distance between lens and source.

Consider now a patch centered on a galaxy cluster of mass M_{500}, our data model for the convergence map at the cluster position is

$$\kappa(\boldsymbol{x}) = U_\kappa(\boldsymbol{x})\kappa_{5\theta_{500}} + n_\kappa(\boldsymbol{x}) \tag{3}$$

with $\theta_{500} \equiv R_{500}/d_L(z)$. $\kappa_{5\theta_{500}}$ is the convergence integrated on a disc of radius $5\theta_{500}$, which can be simply related to the cluster column mass in a cylinder of radius $5R_{500}$, $M_{5R_{500}} = d_L^2\Sigma_{\rm crit}\kappa_{5\theta_{500}}$ [2]. $U_\kappa(\boldsymbol{x})$ is the normalised cluster convergence spatial template, defined as

$$U_\kappa(\boldsymbol{x}) = \frac{\kappa^{\rm true}(\boldsymbol{x})}{\kappa_{5\theta_{500}}} = \left[2\pi\int_0^{5\theta_{500}} dx\, x\, \Sigma(x)\right]^{-1}\Sigma(\boldsymbol{x}), \tag{4}$$

and $n_\kappa(\boldsymbol{x})$ is a stochastic noise term, containing contributions both from the lensing reconstruction noise and from the lensing signal arising from other structures along the line of sight. The latter component is modelled here as a Gaussian field with the standard ΛCDM power spectrum $C_{\kappa\kappa}(\ell)$. A minimum variance estimator for $\kappa_{5\theta_{500}}$ can be obtained as

$$\hat{\kappa}_{5\theta_{500}} = \sigma^2(\hat{\kappa}_{5\theta_{500}})\int d\boldsymbol{\ell} U_\kappa^T(\boldsymbol{\ell})N_{\kappa\kappa}^{-1}(\boldsymbol{\ell})\kappa(\boldsymbol{\ell}), \tag{5}$$

where $N_{\kappa\kappa}$ is the noise power spectrum, $\langle n_\kappa(\boldsymbol{\ell})n_\kappa^*(\boldsymbol{\ell}')\rangle = \delta(\boldsymbol{\ell}-\boldsymbol{\ell}')\,N_{\kappa\kappa}(\boldsymbol{\ell})$, and the variance on $\tilde{\kappa}_{5\theta_{500}}$ is given by

$$\sigma^{-2}(\hat{\kappa}_{5\theta_{500}}) = \int d\boldsymbol{\ell} U_\kappa^T(\boldsymbol{\ell})N_{\kappa\kappa}^{-1}(\boldsymbol{\ell})U_\kappa(\boldsymbol{\ell}). \tag{6}$$

Frequency (GHz)	Noise RMS (μK-arcmin)	Beam FWHM (arcmin)
28	9.8	14.0
41	8.9	10.0
90	1.0	5.0
150	0.9	2.8
230	3.1	2.0

TABLE I: Specifications for a S4 CMB experiment. The frequency bands were chosen to lie on the main atmospheric windows, and the noise levels were designed to yield a map-level rms noise of $\sim 1\mu$K-arcmin after foreground cleaning. The highest and lowest frequency channels could be used to clean dust, cosmic infrared background and synchrotron contamination. In this analysis, we will only include the 41, 90 and 150 GHz channels.

Note that $\sigma^2(\kappa_{5\theta_{500}})$ is linearly related to the variance on the mass measurement

$$\sigma^2(\hat{M}_{5R_{500}}) = \left[d_L^2\,\Sigma_{\rm crit}\right]^2\sigma^2(\hat{\kappa}_{5\theta_{500}}). \tag{7}$$

B. Noise on the convergence maps

Lensing generates off diagonal correlations between different CMB multipoles. The standard approach to reconstruct the convergence field is to form quadratic estimators from the lensed CMB maps $\langle\tilde{X}(\boldsymbol{\ell})\tilde{Y}^*(\boldsymbol{\ell}')\rangle \propto \kappa_{XY}(\boldsymbol{\ell}+\boldsymbol{\ell}')$ [22, 23]. Given a set of experimental specifications (noise level and beam size) it is possible to predict the expected reconstruction noise on the convergence field. We will study two different reconstruction schemes:

- Full reconstruction where the five quadratic estimators $\kappa_{TT}, \kappa_{TE}, \kappa_{TB}, \kappa_{EE}, \kappa_{EB}$ are used to reconstruct the convergence field.
- Polarisation-only reconstruction where we drop all estimators based on the temperature map and use only the polarisation based estimators κ_{EE}, κ_{EB}.

The reason for studying these two different cases is twofold. First, on the smallest angular scales, the level of foreground contamination is higher in temperature than polarisation [24, 25]. When partial foreground cleaning is possible owing to the multifrequency coverage of S4, the leftover systematic effect due to incorrect foreground modeling could hamper the reconstruction. Moreover, the kinematic SZ (kSZ) effect, present mostly in temperature, has the same black-body spectrum as the primordial CMB and can not be subtracted using multifrequency observation. At the level of precision targeted by CMB S4 experiments this could lead to significant biases in the convergence map. The second reason for ignoring the temperature-based estimators is atmospheric noise. Since the likely implementation of S4 will be in the form of a set of ground-based facilities, the largest

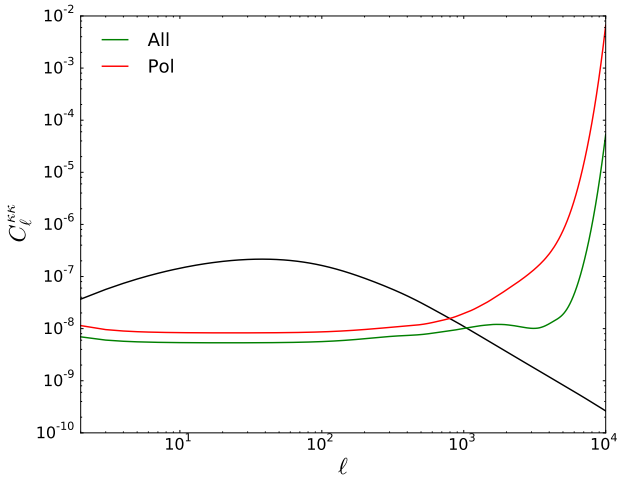

FIG. 1: Lensing noise for the two minimum variance combinations highlighted in the text, containing all two-point combinations (green) and polarisation-only combinations (red). The CMB lensing convergence power spectrum is shown as a black solid line. The noise curves correspond to the survey specifications in Table I.

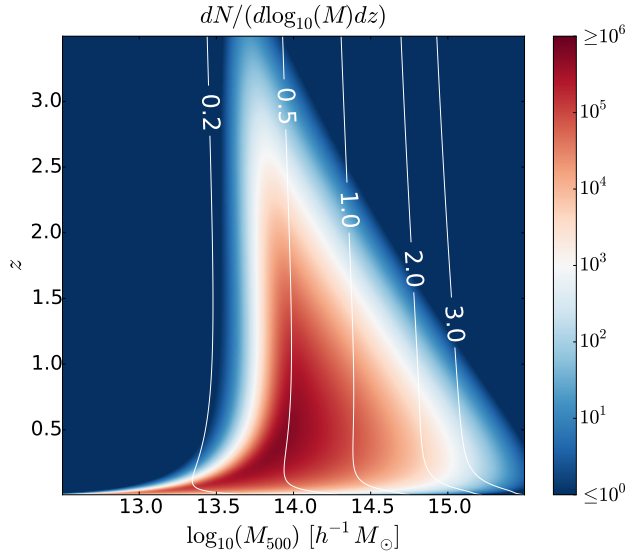

FIG. 2: Mass and redshift distribution of tSZ detected clusters for a CMB S4 experiment, the contour lines correspond to the signal to noise on the mass measurement of each individual cluster using CMB lensing estimated from polarisation data.

angular scales will suffer from contamination due to atmospheric emission (see for example Figure 2 of [26]). While the exact level of this atmospheric contamination will depend on the geographical location of S4, as well as on its scanning strategy, we choose to follow a conservative approach presenting as a baseline the results for polarisation-only estimators, where atmospheric contamination is smaller and can be mitigated through the use of half-wave plates [27]. Considering polarisation-only estimators further allows us to fully decouple the measurements of the cluster convergence and thermal Sunyaev-Zel'dovich effect.

The experiment specifications of S4 assumed here are reported in Table I. The frequency channels were chosen to lie on the atmospheric windows, the relative noise levels were defined assuming template foreground cleaning from synchrotron at low frequencies (spectral index $\beta_s = -3$) and from thermal dust emission at high frequencies (spectral index $\beta_d = 1.5$). The absolute noise scale was chosen to yield a map-level RMS noise of 1μK-arcmin, and the beam widths correspond to a 3m aperture telescope. We further assume a total surveyed area of $f_{\rm sky} = 0.4$. The lensing noise corresponding to the two minimum-variance combinations (with and without temperature information) for these specifications are shown in Fig. 1, and were computed using `quicklens`[44].

III. CALIBRATION OF THE $Y - M$ RELATIONSHIP

In this section, we discuss the tight scaling relationship between the integrated tSZ flux Y emitted by a cluster and its mass, and how to calibrate this relationship using measurements of cluster gravitational lensing. We start by discussing our method to estimate the statistics of the cluster sample achievable with S4, which determines the accuracy with which this relationship can be constrained. We then consider the empirical $Y - M$ scaling relation

$$Y_{500} = \tilde{A}_Y \left[\frac{d_A(z)}{100\,{\rm Mpc}/h}\right]^{-2} \left[\frac{(1-b)M_{500}}{1.5\times10^{14}\,M_\odot/h}\right]^{\alpha_Y} E^{3/2}(z), \quad (8)$$

where d_A is the angular diameter distance to the cluster, $\alpha_Y = 1.79$, $\tilde{A}_Y = 5.0\times10^{-10}{\rm sr}^2$, and $E(z) \equiv H(z)/H_0$ [2]. We will present forecasts for constraints on the hydrostatic parameter b, on a generic power-law model and on a non-parametric mass- and redshift-dependent $Y-M$ relationship.

A. Cluster detection

The tSZ effect arises due to inverse Compton scattering of CMB photons with the hot electron gas inside clusters, it results in secondary contributions to the CMB anisotropies [28]

$$\left.\frac{\Delta{\rm T}}{\rm T}\right|_{\rm tSZ}(\nu,\boldsymbol{x}) = f_{\rm tSZ}(\nu)\frac{\sigma_T}{m_e c^2}\int P_e(l,\boldsymbol{x})\,dl \equiv f_{\rm tSZ}(\nu)\,y(\boldsymbol{x}), \quad (9)$$

where $P_e = k_{\rm B} n_e T_e$ is the electron pressure, σ_T is the Thomson scattering cross-section, and where we have defined the dimensionless Compton-y parameter, $y(\boldsymbol{x})$.

The spectral signature of the tSZ effect $f_{\rm tSZ}(\nu)$ allow us to separate it from other types of emission in microwave frequency bands. We start by defining the cluster detection efficiency

$$\tilde{\chi}(M_{500},z) = \int d(\ln Y_{500}^{\rm true}) \int_{q\sigma_N}^{\infty} dY_{500}^{\rm obs} \\ P_{\rm SZ}(\ln Y_{500}^{\rm true}|M_{500},z)\, P_{\rm det}(Y_{500}^{\rm obs}|Y_{500}^{\rm true}), \quad (10)$$

where $P_{\rm det}$ is the probability of obtaining a measurement $Y_{500}^{\rm obs}$ for a true integrated tSZ flux $Y_{500}^{\rm true}$, and $P_{\rm SZ}$ is the distribution of integrated tSZ fluxes for clusters of mass M_{500} at redshift z, which accounts for the intrinsic scatter in the $Y-M$ relation. We have defined the tSZ flux Y_{500} as the normalised integral of the cluster pressure profile on a sphere of radius R_{500}. We refer the reader to Appendix A of [29] for a precise definition of Y_{500} as well as the formalism used to model the tSZ catalog achievable by S4.

The detection efficiency is determined by the noise in the Y-measurements. For this, and following [29], we used a matched-filter approach, which allows us to obtain optimal uncertainties simulaneously marginalised over the amplitude of the kSZ effect. We find that S4 will be able to produce a catalog with $\sim 2\times10^5$ clusters for a tSZ signal-to-noise threshold $q_Y > 6$, two orders of magnitude above what is available today. With such a large number of sources, a number of them will inevitably overlap on the sky, complicating the accurate measurement of their individual tSZ or lensing signatures. In order to determine the magnitude of this problem we start by defining the radius $\theta_{\rm blend}$ as the aperture containing 95% of the beam-convolved pressure profile for the typical cluster size in the catalog. We then use this value to estimate the fraction of clusters that overlap with other sources within $\theta_{\rm blend}$ to be $f_{\rm blend}\sim 0.25$. In the rest of this analysis we therefore remove 25% of the cluster sample. Note that this is a conservative approach, since blended sources could in principle be disentangled given an accurate model of their profiles. The mass and redshift distribution of the resulting catalog, as well as the signal-to-noise on individual cluster masses measured with CMB lensing are shown in Fig. 2. The S/N increases with cluster mass but is not strongly dependent on its redshift.

In the following, we will assume that each cluster in the catalog experiment has a counterpart in an overlapping spectroscopic or photometric galaxy survey, and that the errors on the redshift of individual clusters can be neglected. CMB S4 is currently designed to have a full overlap with LSST [30] and 4MOST [31], and while redshift uncertainties might play a role in the calibration of the $Y-M$ relationship, they are always subdominant compared to uncertainties in the cluster mass inferred from gravitational lensing.

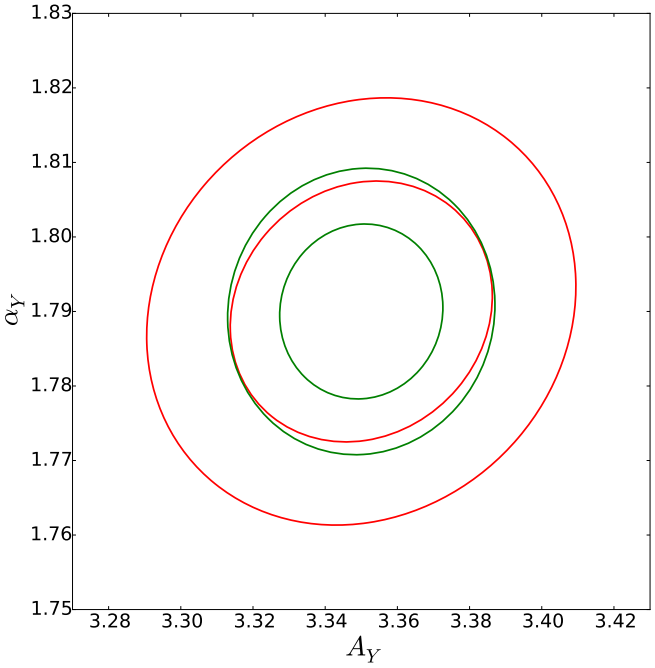

FIG. 3: Constraints on the parameters of the $Y-M$ scaling relationship for CMB S4 experiment. The 1 and 2σ contours are displayed. In green we show the result for the full reconstruction of the convergence field and in red the result based on polarisation data only.

B. Hydrostatic bias

As was mentioned in Section I, cluster masses inferred from X-ray observations can be biased due to the assumption of hydrostatic equilibrium (HE). This effect can be taken into account by introducing the hydrostatic bias parameter: $M_Y = M_{500}^{\rm HE} = (1-b)M_{500}$. Gravitational lensing of the CMB provides an unbiased way of measuring cluster masses $M_L = M_{500}$ and can be used to put a prior on b [2].

The two mass measurements uncertainties are

$$\frac{\sigma^2(M_Y)}{(M_Y)^2} = \alpha_Y^2 \frac{\sigma^2(Y_{500})}{Y_{500}^2}, \quad \frac{\sigma^2(M_L)}{(M_L)^2} = \frac{\sigma^2(\kappa_{5\theta_{500}})}{\kappa_{5\theta_{500}}^2} \quad (11)$$

The relative error on $\epsilon = (1-b)$ for a single cluster is then given by:

$$\frac{\sigma^2(\epsilon)}{\epsilon^2} = \frac{\sigma^2(M_Y)}{(M_Y)^2} + \frac{\sigma^2(M_L)}{(M_L)^2} \\ = \alpha_Y^2 \frac{\sigma^2(Y_{500})}{Y_{500}^2} + \frac{\sigma^2(\kappa_{5\theta_{500}})}{\kappa_{5\theta_{500}}^2}. \quad (12)$$

Assuming independent estimates for each cluster, the un-

certainty for the total cluster sample is:

$$\left[\frac{\sigma(\epsilon)}{\epsilon}\right]^{-2}_{\rm tot} = \sum_{i=1}^{N_c}\left[\frac{\sigma_i(\epsilon)}{\epsilon}\right]^{-2} = \int dz \frac{dV}{dz}\int dM \frac{n(M,z)\tilde{\chi}(M,z)}{\sigma^2(\epsilon)\epsilon^{-2}(M,z)}, \quad (13)$$

where $dV/dz \equiv 4\pi\, f_{\rm sky}\, c\, r^2(z)/H(z)$ is the derivative of the comoving volume as a function of redshift, and $n(M,z)$ is the halo mass function (comoving number density of haloes in a differential bin of mass).

The relative uncertainties corresponding to the two different lensing reconstruction schemes described Section II B are

$$\frac{\sigma(\epsilon)}{\epsilon} = 2.51\times10^{-3} \quad \text{(Temp.+Pol.)} \quad (14)$$

$$\frac{\sigma(\epsilon)}{\epsilon} = 3.97\times10^{-3} \quad \text{(Pol. only)}. \quad (15)$$

Cluster lensing of the CMB therefore allows us to constrain the hydrostatic bias parameter to sub-percent accuracy. This is useful, not only as a strong prior when extracting cosmological constraints from cluster number counts, but also as a source of information on cluster gas physics. In this computation we have fixed all parameters of the scaling relationship, assuming that X-ray observations could be used to put strong priors on them. In the following we will show that lensing measurements by CMB S4 could be used to constrain these parameters directly.

C. Scaling relation calibration

In this section we explore the possibility of using CMB lensing alone to constrain the $Y-M$ relationship, thus bypassing the need for X-ray follow-up observations and the uncertainties associated with the hydrostatic bias. We start by parametrising the $Y-M$ relationship as a scaling law

$$\frac{Y_{500}}{10^{-10}\,{\rm srad}} = E^{2/3}(z)\left(\frac{100\,{\rm Mpc}/h}{d_A(z)}\right)^2 A_Y\left(\frac{M_{500}}{M_*}\right)^{\alpha_Y}, \quad (16)$$

with pivot scale $M_* = 1.5\times10^{14}M_\odot\, h^{-1}$.

We use a Fisher matrix formalism to predict the uncertainties on the amplitude A_Y and the power law index α_Y. These come from three sources: the measurement uncertainties on the tSZ flux, the intrinsic scatter in the $Y-M$ relationship and uncertainties on the cluster lensing mass measurement. The first two sources of uncertainty are always subdominant compared to the later, and in this section we will assume that they can be neglected. A joint likelihood formalism that consistently accounts for all sources of uncertainty will be presented in Section IV. Within this approximation and assuming Gaussian measurement errors, the form of the likelihood is simple

$$-\ln\mathcal{L} \propto \sum_{i=1}^{N_c}\frac{\left[M^{obs}_{500,i} - f(Y_{500,i},A_Y,\alpha_Y)\right]^2}{2\sigma^2_{M_{500,i}}}, \quad (17)$$

where $f(Y_{500},A_Y,\alpha_Y)\equiv M_{500}(Y_{500},A_Y,\alpha_Y)$ is given in Eq. 8. The Fisher matrix therefore takes a simple form:

$$F_{\alpha\beta} = \int dz\frac{dV}{dz}\int dM\frac{n(M,z)\tilde{\chi}(M,z)}{\sigma^2(M,z)}\frac{\partial f}{\partial\alpha}\frac{\partial f}{\partial\beta},$$

and all terms of the Fisher matrix can be computed analytically.

Fig. 3 shows the resulting constraints for a S4 CMB experiment where we consider the full reconstruction of the convergence map as well as the reconstruction based on polarisation-only data. The power-law index α_Y and the amplitude A_Y could be measured at the per-cent level, using only CMB data.

D. Non-parametric reconstruction of the Y-M relationship

The high accuracy on the calibration of the $Y-M$ scaling relation for CMB S4 experiments ($>200\sigma$ determination of the hydrostatic bias) leads us to investigate a non-parametric reconstruction of the $Y-M$ relation. The main interest of this approach is the avoidance of a particular modelling prior.

Let us start by defining the redshift-independent observable $\mathcal{Y} = d_A^2 Y_{500}/E^{2/3}(z)$. We define a non-parametric relation between $\mathcal{Y}$ and M in N_b bins of $\mathcal{Y}$ characterised by edges $[\mathcal{Y}^i_n,\mathcal{Y}^f_n]$ ($n\in[1,N_b]$) as:

$$M(\mathcal{Y}) = \sum_n M_n\, W(\mathcal{Y}|\mathcal{Y}^i_n,\mathcal{Y}^f_n), \quad (18)$$

where $W(x|x_a,x_b)$ is a top-hat window function in the interval $[x_a,x_b]$.

Under the assumption that the uncertainty in the lensing mass measurement dominates over the uncertainty on $\mathcal{Y}$ (which receives contributions from the measurement uncertainties as well as the intrinsic scatter), and following the same χ^2 argument used in the previous section, we can compute the expected errors on M_n as

$$\sigma^{-2}(M_n) = \int dz\frac{dV}{dz}\int_{M^0_n}^{M^f_n} dM\frac{n(M,z)\tilde{\chi}(M,z,b)}{\sigma^2(M_L)}. \quad (19)$$

Figure 4 shows the 1σ uncertainties on this $\mathcal{Y}-M$ relationship for $N_b=44$ logarithmic bins of mass in the range $M\in[2\times10^{13},2\times10^{15}]\,M_\odot/h$, as well as the signal-to-noise ratio in each bin. Note that while we illustrate the method assuming a simple power-law relation between $\mathcal{Y}$ and M, the error on each mass bin is independent of this particular choice, and thus this method could be used

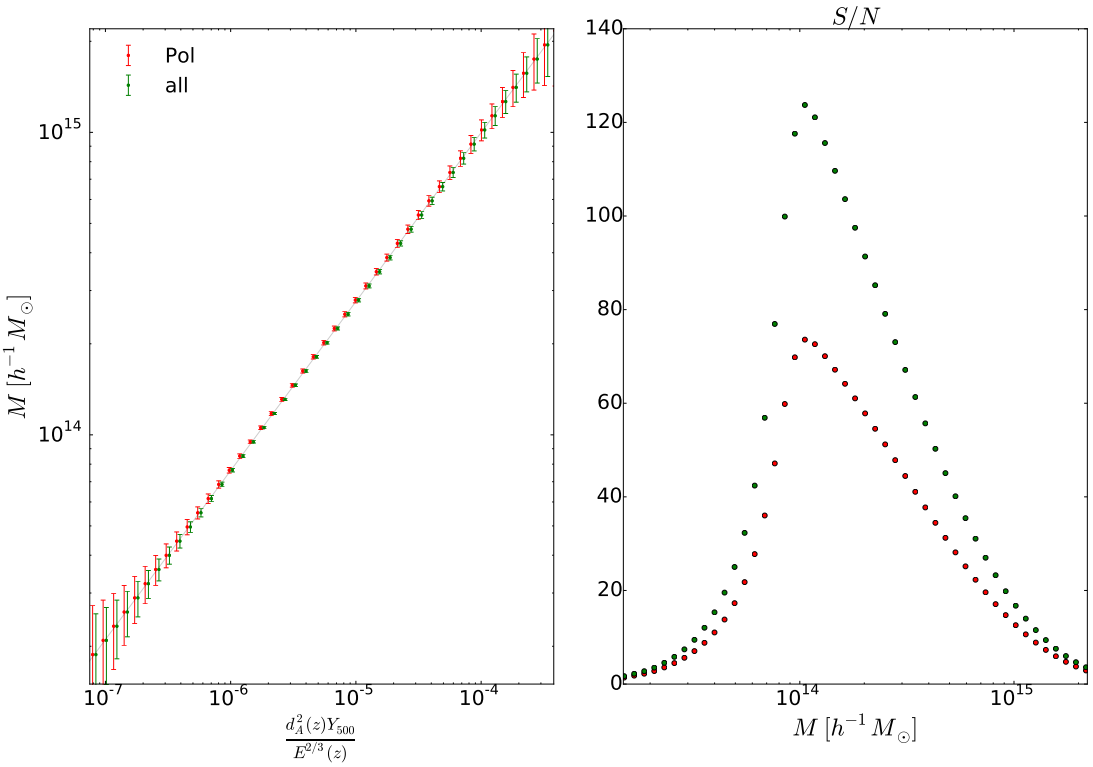

FIG. 4: Non-parametric reconstruction of the $\mathcal{Y} - M$ relationship using estimate of the convergence field from the polarised CMB. The left panel shows the error bars on the scaling relation, the right panel shows the S/N for each of the 44 mass bins. Note that the S/N will depend on the exact choice of model that is assumed for the relationship. Results are shown in green for the minimum variance lensing reconstruction and in red for reconstruction using only polarisation-based estimators.

to detect deviations from this fiducial model, providing significant insight into the physics of clusters. The S/N is a function of the number of cluster detected inside a given mass bin and the error on the reconstruction of the convergence field. A CMB S4 experiment would be able to reconstruct the cluster $Y - M$ relation with $S/N > 5$ for 38 bins in the mass range $[2.9\times10^{13}, 1.5\times10^{15}]M_\odot/h$, peaking at masses $\sim 10^{14}M_\odot/h$ using measurements of the lensing signal from polarisation data only.

This method can, also be used to study the redshift dependence of the $Y-M$ relation. As an example, Figure 5 shows the possible constraints on the non-parametric model in 7 different bins of redshift in the range $0 \leq z \leq 3.2$. Significant constraints on the scaling relationship can still be drawn in this case in a wide range of masses for all redshifts.

IV. JOINT CONSTRAINTS FROM TSZ AND LENSING MEASUREMENTS

The aim of this section is to provide a general formalism to consistently account for the uncertainties in the $Y - M$ relation when drawing cosmological constraints from cluster number counts. This is of particular interest in the presence of lensing data which, as we have seen, can directly constrain this relation. Assuming that we have measured the redshift z, tSZ flux $Y_{\rm obs}$ and lensing mass M_L for each cluster in the catalog, we use as our basic observable the number of clusters detected in bins of these three quantities:

$$\frac{N(q, M_L, z)}{\Delta q_Y\,\Delta M_L\,\Delta z} \equiv \int dM dY \frac{d^3N}{dz\,dM\,dY} P(q_Y, M_L|Y, M), \tag{20}$$

where $P(q_Y, M_L|Y, M)$ is the probability of measuring a lensing mass M_L and a tSZ flux with a signal-to-noise $q_Y \equiv Y_{\rm obs}/\sigma_Y$ for a cluster of true mass M and tSZ flux Y. Note that we have chosen to use q_Y instead of $Y_{\rm obs}$ as the observable variable, since the fiducial cluster catalog assumed here is defined by a threshold $q_Y > 6$. We proceed by making the following assumptions:

1. The tSZ and lensing measurements are independent, and the noise on these quantities has a Gaussian distribution. In this case we can write:

$$P(q_Y, M_L|Y, M) = \mathcal{N}(q_Y|Y/\sigma_Y, 1)\,\mathcal{N}(M_L|M, \sigma_\kappa), \tag{21}$$

where $\mathcal{N}(x|\mu, \sigma)$ is the normal distribution with mean μ and variance σ^2, and σ_Y and σ_L are the errors in the measurement of $Y_{\rm obs}$ and M_L.

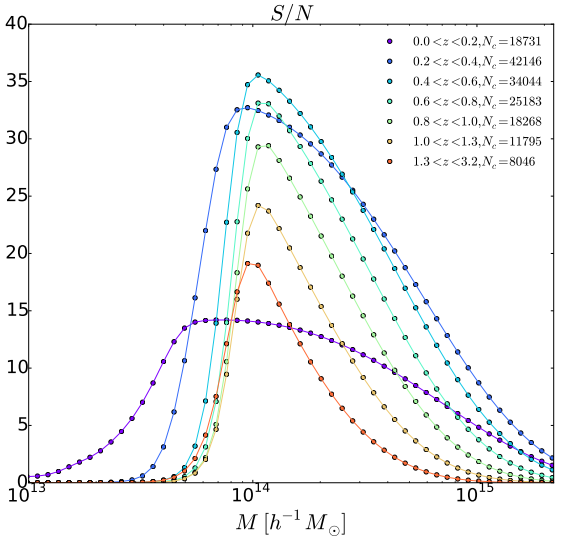

FIG. 5: S/N on the reconstruction of the $\mathcal{Y}-M$ in seven bins of redshift. A S4 CMB experiment will be able to measure the redshift evolution of this scaling relation to good accuracy in a wide range of masses. The number of clusters found in each redshift bin is indicated in the legend. The masses are estimated using only polarisation-based estimators.

2. The true tSZ flux and halo mass are related through a stochastic log-normal model, such that $\log Y = \log \bar{Y}(M,z) + n_Y$, where n_Y is a random normal variable with mean 0 and standard deviation $\sigma_{\log Y}$. $\bar{Y}(M,z|\mathbf{p})$ is a scaling relation dependent on a set of nuisance parameters $\mathbf{p}$ that we will specify later on. We can then write

$$\frac{d^3N}{dz\,dM\,d\log Y} = \frac{dN^2}{dz\,dM}\,\mathcal{N}(\log Y|\log\bar{Y},\sigma_{\log Y}), \quad (22)$$

where

$$\frac{d^2N}{dzdM} = 4\pi f_{\rm sky}\,\frac{c\,r^2(z)}{H(z)}\,n(M,z) \quad (23)$$

and $n(M,z)$ is the halo mass function.

3. Finally, we assume that the fluctuations in the counts of objects in different bins of q_Y, z and M_L are independent and Poisson-distributed, such that the likelihood for a given set of counts $N_{\rm obs}$ is:

$$\ln\mathcal{L}(N_{\rm obs}|\bar{N}) = \sum_{z,q_Y,M_L}\left[N_{\rm obs}\,\ln\bar{N} - \bar{N} - \ln(N_{\rm obs}!)\right]_{z,q_Y,M_L} \quad (24)$$

where $\bar{N}(z,q_Y,M_L)$ is the mean number of clusters given above, which depends both on the cosmological parameters and the $Y-M$ relation.

Expanding Eq. 24 around the maximum likelihood point, we find the expression for the Fisher matrix [32]:

$$F_{\alpha\beta} = \sum_{z,q_Y,M_L}\frac{\partial_\alpha\bar{N}(z,q_Y,M_L)\,\partial_\beta\bar{N}(z,q_Y,M_L)}{\bar{N}(z,q_Y,M_L)}. \quad (25)$$

We can then produce forecasts for cosmological constraints from number counts consistently marginalised over the $Y-M$ relation by computing the Fisher matrix above including both the cosmological parameters and the mass calibration parameters $\mathbf{p}$. For this analysis we will use a generalised version of the simple scaling relation 8 to account for additional variation with respect to mass and redshift:

$$E^{-2/3}(z)\left[\frac{d_A}{100\,{\rm Mpc}/h}\right]^2\frac{\bar{Y}(M,z)}{10^{-10}\,{\rm srad}} = A_Y\left(\frac{M}{M_*}\right)^{\alpha_Y} e^{\beta_Y\log^2(M/M_*)}(1+z)^{\gamma_Y}. \quad (26)$$

The set of nuisance parameters for this model is therefore $\mathbf{p} \equiv (A_Y,\alpha_Y,\beta_Y,\gamma_Y,\sigma_{\log Y})$, for which we will use the fiducial values reported in [2]: $\mathbf{p} = (3.35\times10^{-10}{\rm srad}^2, 1.79, 0, 0, 0.127)$ (for a pivot scale $M_* = 1.5\times10^{14}\,M_\odot\,h^{-1}$).

We produce constraints for a cluster sample divided into 64 logarithmic bins of q_Y and M_L in the ranges $q_Y\in[6,500]$, $\log_{10}M_\kappa/(M_\odot\,h^{-1})\in[12.5,15.5]$, and 10 bins of redshift between $z=0$ and $z=2$. Note that in principle it should be possible to use much narrower redshift intervals, however we choose to use wide bins ($\Delta z = 0.2$) to justify using a purely Poisson likelihood, ignoring the sample covariance caused by the average fluctuation of the density field inside each bin [33].

In order to include in our forecasts the cosmological constraints achievable with other complementary probes, we have also carried out a Fisher matrix forecast for measurements of the CMB primary and lensing power spectra using the formalism described in [34]. In this case we have considered two experimental setups, corresponding to S4 as described in Table I, and to the Planck experiments [35], modelled assuming a map-level RMS noise of 43μK-arcmin, a Gaussian beam of 7 arcmin FWHM and a sky fraction $f_{\rm sky}=0.7$. In both cases we impose a maximum ℓ cut of $\ell_{\rm max}=3000$ in intensity and $\ell_{\rm max}=5000$ in polarisation, and in the case of S4 we assume a minimum ℓ cut of $\ell_{\rm min}=30$. When combining both experiments we assume S4-only and Planck-only constraints on 40% and 30% of the sky respectively for $\ell>30$, and Planck-only constraints on 70% of the sky for $2<\ell<30$. The resulting Fisher matrix is then directly added to the Fisher matrix for cluster number counts computed as described above, under the assumption that the constraints from both probes are uncorrelated. In all cases we marginalise over a set of 7 cosmological parameters: the matter density parameter Ω_m, the baryon fraction $f_b\equiv\Omega_b/\Omega_M$, the Hubble parameter h, the scalar spectral index n_s and amplitude A_s, the optical depth τ and the sum of neutrino masses $\sum m_\nu$. For these parameters we use the fiducial values mentioned in Section I, as well as the value $\sum m_\nu = 60\,{\rm meV}$, corresponding to the lower limit allowed by neutrino oscillation experiments. Together with the cluster nuisance parameters introduced above we therefore consider a 12-dimensional parameter

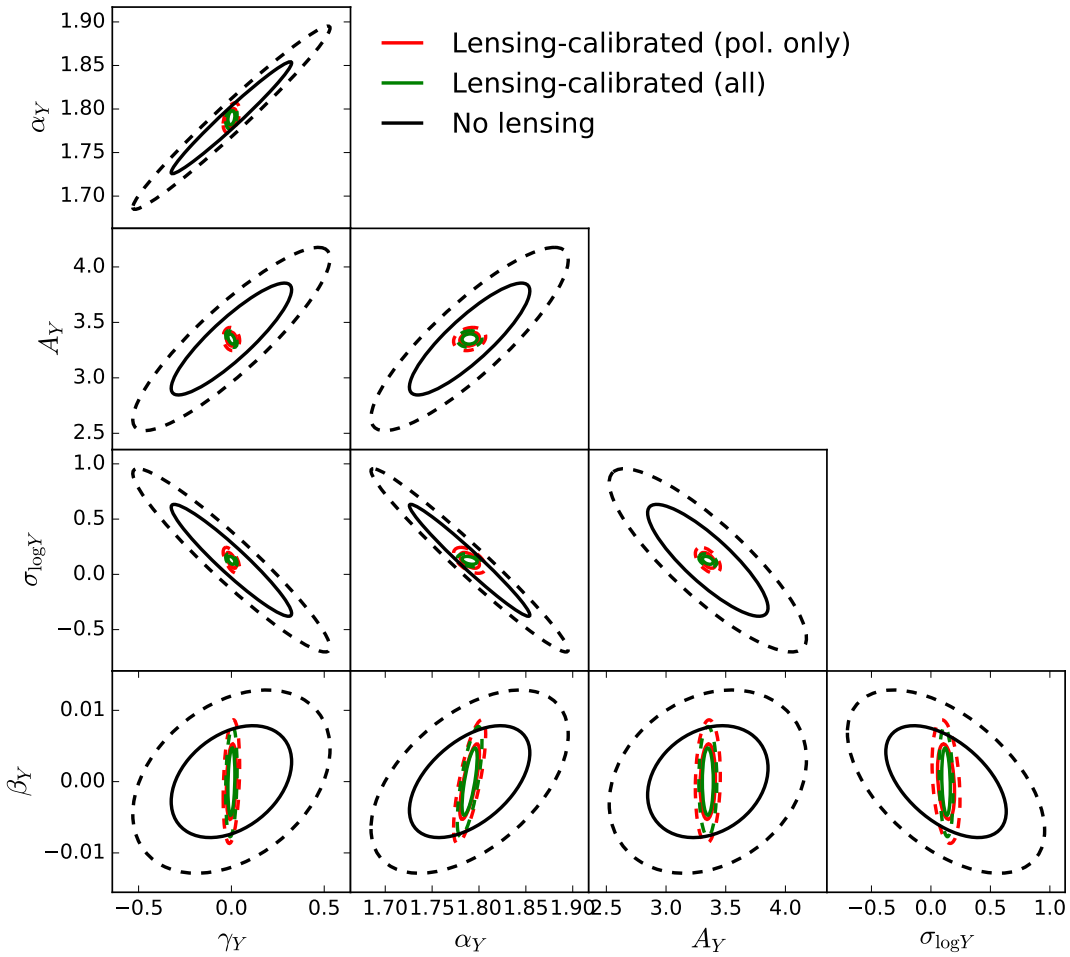

FIG. 6: Uncertainties on the cluster nuisance parameters marginalised over the cosmological parameters for an SZ survey carried out with S4 without lensing information (black ellipses), with lensing masses reconstructed using only polarisation information (red ellipses) and using also temperature (green ellipses). In all cases we include prior information on the cosmological parameters from Planck.

space. Power spectra were computed using the public code `CLASS` [36].

The red and green ellipses in Figure 6 show the constraints on the nuisance parameters of the scaling relation for lensing mass measurements carried out using polarisation-only quadratic estimators, and all estimators respectively. The constraints are marginalised over all cosmological parameters, and show the small effect of discarding temperature data on the cluster parameters. It is worth pointing out that, even in the absence of mass measurements it would be possible to constrain the parameters of the $Y-M$ relation to some extent, since they affect the observed cluster mass distribution, which is independently constrained from N-body simulations. The achievable constraints in the absence of cluster lensing masses are represented by the black ellipses in the same figure. The effect of cluster lensing information on the constraints for the most relevant cosmological parameters is shown in Figure 7 using the same color code. Of particular relevance is the factor ~ 3.3 improvement in the uncertainty on the sum of neutrino masses, a key science case for S4. We further showcase the role of cluster number counts in constraining this parameter in Figure 8. While the constraints on $\sum m_\nu$ from cluster abundances alone are irrelevant given current bounds, and achievable constraints with S4 in combination with Planck using only power spectrum information would not yield a significant measurement of neutrino masses, the combination of both probes can efficiently break degeneracies between different cosmological parameters, enabling a $\sim 5\sigma$ measurement of $\sum m_\nu$ ($\sigma(\sum m_\nu) = 13.2\,\mathrm{meV}$) when using lensing mass information to constrain the $Y-M$ relation.

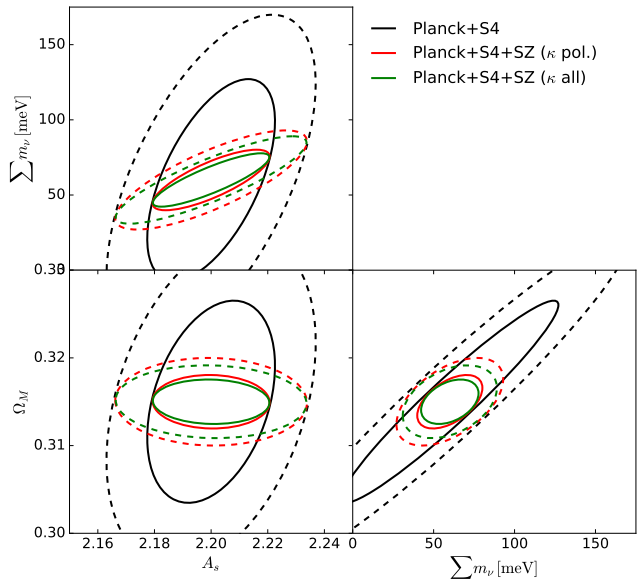

FIG. 7: Uncertainties Ω_M, A_s and the sum of neutrino masses from an SZ catalog carried out with S4 in combination with constraints from S4 primary and lensing power spectra, as well as Planck temperature and polarisation on $\ell < 30$. Results are shown in the absence of lensing mass estimates (black ellipses), and for lensing masses computed using only polarisation (red ellipses) and temperature and polarisation (green ellipses). The results are marginalised over all other cosmological parameters as well as the cluster nuisance parameters.

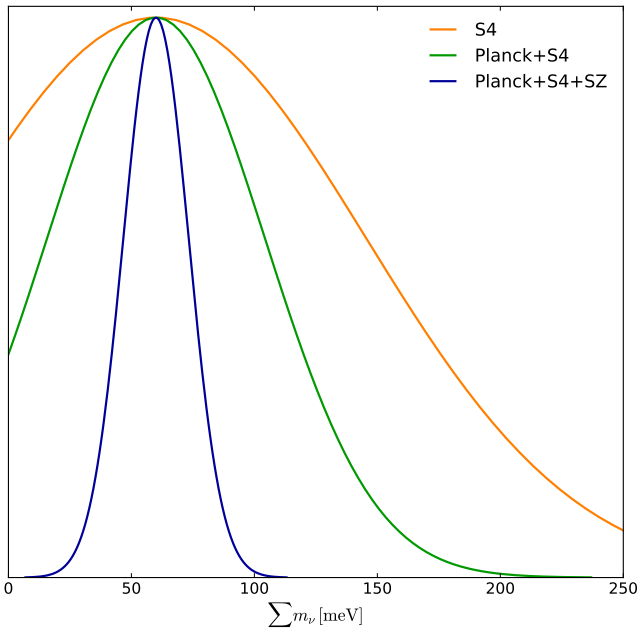

FIG. 8: Posterior distribution for the sum of neutrino masses for different experiment configurations: S4 primary and lensing power spectra (gray curve), S4 power spectra and Planck primary on $\ell < 30$ (orange curve), S4 and Planck power spectra together with SZ number counts from S4 in the absence of lensing masses (green curve) and for lensing masses measured using only polarisation information (blue curve).

V. DISCUSSION

We have studied the potential of using CMB lensing by clusters to calibrate their masses in the era of CMB Stage-4 experiments. We have found that CMB S4 will allow a sub-percent determination of the hydrostatic bias parameter relating the mass inferred from X-ray observation to the true cluster mass. We have then extended the model and shown that the large number of detected clusters and the low uncertainties in the reconstructed convergence maps could be used to calibrate the $Y - M$ relationship using solely CMB data. We have also studied the constraints on a non-parametric reconstruction of the $Y - M$ relationship which can be used to study the evolution of this relation with mass and redshift with high significance over a wide range of masses. Throughout the paper we have studied the impact of discarding temperature data in the reconstruction of the convergence field. This is an important comparison, since the temperature data from Stage-4 CMB experiments will suffer from atmospheric contamination and residual foregrounds. Finally we have presented a joint likelihood for tSZ and lensing mass measurements allowing us to forecast constraints on cosmological parameters while consistently accounting for the uncertainties in the $Y - M$ scaling relation.

The method presented here relies on a number of assumptions. Testing and characterising the effect of each of these assumptions is the subject of future work but it is worth quoting the following caveats, which might affect future analyses with real data:

- Throughout this paper, we have modelled the lensing field and the lensing reconstruction noise as Gaussian fields. At the level of precision achieved by CMB Stage-4 experiments this assumption may break down [37, 38], and the non-Gaussian contribution to the signal and/or the noise should be studied in detail.

- We used a Poisson likelihood for cluster number counts. While this is commonly used for current cluster catalogs, the high number of clusters detected in the CMB S4 catalog might require a more sophisticated treatment. Studies of possible departure from Poisson for cluster number count can be found in [33, 39, 40], where a sample variance term is added to the Poisson shot-noise term to account for the fact that cluster are peaks of the same underlying density field. In our analysis we have used wide redshift bins to reduce the impact of sample variance.

- We have not included the covariance between the CMB lensing power spectrum and cluster counts calibrated using CMB lensing when constraining cosmological parameters. In practice, the full covariance could be constructed from Monte-Carlo

simulations while analysing CMB S4 data (e.g. see [41]).

- The cluster mass function used to determine cosmological parameters is a fit to N-body simulations [16]. In order to achieve the accuracy required for S4, in particular for non-standard scenarios such as massive neutrinos [42], a better understanding of the theoretical uncertainties in the mass function is necessary, in particular regarding the effects of baryonic physics [43].

- Finally, we have assumed knowledge of the cluster mass [21] and pressure [6] profiles, and this assumption allows us to devise a minimum-variance estimate of Y and M from the data. However, this needs to be validated using hydrodynamic simulations at the level of precision corresponding to the uncertainties on cosmological parameters. A more careful analysis of cluster de-blending is also necessary

While more work need to be done to address each of these issues, we have shown that using cluster lensing to calibrate cluster masses has an important potential and could play a role in the future determination of the sum of neutrinos masses. This, combined with particle physics measurements, could allow us to distinguish between the normal and inverted hierarchies, thus opening a new window on fundamental physics.

Acknowledgments

We thank Nicholas Battaglia, Joanna Dunkley, Pedro Ferreira, Mathew Madhavacheril, Sigurd Næss and Joseph Silk, for useful comments and discussions. TL is supported by ERC grant 267117 (DARK) hosted by Universite Pierre et Marie Curie- Paris 6 and by the Labex ILP (reference ANR-10-LABX-63) part of the Idex SUPER, and received financial state aid managed by the Agence Nationale de la Recherche, as part of the programme Investissements d'avenir under the reference ANR-11-IDEX-0004-02. DA is supported by the Beecroft Trust and ERC grant 259505.

[1] Planck Collaboration, P. A. R. Ade, N. Aghanim, M. Arnaud, M. Ashdown, J. Aumont, C. Baccigalupi, A. J. Banday, R. B. Barreiro, R. Barrena, et al., ArXiv e-prints (2015), 1502.01598.
[2] Planck Collaboration, P. A. R. Ade, N. Aghanim, M. Arnaud, M. Ashdown, J. Aumont, C. Baccigalupi, A. J. Banday, R. B. Barreiro, J. G. Bartlett, et al., ArXiv e-prints (2015), 1502.01597.
[3] M. Bonamente, M. Joy, S. J. LaRoque, J. E. Carlstrom, D. Nagai, and D. P. Marrone, Astrophys. J. **675**, 106-114 (2008), 0708.0815.
[4] D. P. Marrone, G. P. Smith, N. Okabe, M. Bonamente, J. E. Carlstrom, T. L. Culverhouse, M. Gralla, C. H. Greer, N. Hasler, D. Hawkins, et al., Astrophys. J. **754**, 119 (2012), 1107.5115.
[5] C. Sifón, F. Menanteau, M. Hasselfield, T. A. Marriage, J. P. Hughes, L. F. Barrientos, J. González, L. Infante, G. E. Addison, A. J. Baker, et al., Astrophys. J. **772**, 25 (2013), 1201.0991.
[6] M. Arnaud, G. W. Pratt, R. Piffaretti, H. Böhringer, J. H. Croston, and E. Pointecouteau, A&A **517**, A92 (2010), 0910.1234.
[7] Planck Collaboration, P. A. R. Ade, N. Aghanim, C. Armitage-Caplan, M. Arnaud, M. Ashdown, F. Atrio-Barandela, J. Aumont, C. Baccigalupi, A. J. Banday, et al., A&A **571**, A20 (2014), 1303.5080.
[8] R. Piffaretti and R. Valdarnini, A&A **491**, 71 (2008), 0808.1111.
[9] D. Nagai, A. V. Kravtsov, and A. Vikhlinin, Astrophys. J. **668**, 1 (2007), astro-ph/0703661.
[10] M. Meneghetti, E. Rasia, J. Merten, F. Bellagamba, S. Ettori, P. Mazzotta, K. Dolag, and S. Marri, A&A **514**, A93 (2010), 0912.1343.
[11] R. E. Angulo, V. Springel, S. D. M. White, A. Jenkins, C. M. Baugh, and C. S. Frenk, MNRAS **426**, 2046 (2012), 1203.3216.
[12] M. Madhavacheril, N. Sehgal, R. Allison, N. Battaglia, J. R. Bond, E. Calabrese, J. Caliguiri, K. Coughlin, D. Crichton, R. Datta, et al., Physical Review Letters **114**, 151302 (2015), 1411.7999.
[13] E. J. Baxter, R. Keisler, S. Dodelson, K. A. Aird, S. W. Allen, M. L. N. Ashby, M. Bautz, M. Bayliss, B. A. Benson, L. E. Bleem, et al., Astrophys. J. **806**, 247 (2015), 1412.7521.
[14] J.-B. Melin and J. G. Bartlett, A&A **578**, A21 (2015), 1408.5633.
[15] Planck Collaboration, P. A. R. Ade, N. Aghanim, M. Arnaud, M. Ashdown, J. Aumont, C. Baccigalupi, A. J. Banday, R. B. Barreiro, J. G. Bartlett, et al., ArXiv e-prints (2015), 1502.01589.
[16] J. Tinker, A. V. Kravtsov, A. Klypin, K. Abazajian, M. Warren, G. Yepes, S. Gottlöber, and D. E. Holz, Astrophys. J. **688**, 709-728 (2008), 0803.2706.
[17] U. Seljak and M. Zaldarriaga, Astrophys. J. **538**, 57 (2000), astro-ph/9907254.
[18] M. Zaldarriaga and U. Seljak, Phys. Rev. D **59**, 123507 (1999), astro-ph/9810257.
[19] G. Holder and A. Kosowsky, Astrophys. J. **616**, 8 (2004), astro-ph/0401519.
[20] C. Vale, A. Amblard, and M. White, **10**, 1 (2004), astro-ph/0402004.
[21] J. F. Navarro, C. S. Frenk, and S. D. M. White, Astrophys. J. **462**, 563 (1996), astro-ph/9508025.
[22] W. Hu and T. Okamoto, Astrophys. J. **574**, 566 (2002), astro-ph/0111606.
[23] A. Lewis and A. Challinor, Physics Reports **429**, 1 (2006), astro-ph/0601594.
[24] S. Naess, M. Hasselfield, J. McMahon, M. D. Niemack,

G. E. Addison, P. A. R. Ade, R. Allison, M. Amiri, N. Battaglia, J. A. Beall, et al., JCAP **10**, 007 (2014), 1405.5524.
[25] A. T. Crites, J. W. Henning, P. A. R. Ade, K. A. Aird, J. E. Austermann, J. A. Beall, A. N. Bender, B. A. Benson, L. E. Bleem, J. E. Carlstrom, et al., Astrophys. J. **805**, 36 (2015), 1411.1042.
[26] S. Das, T. Louis, M. R. Nolta, G. E. Addison, E. S. Battistelli, J. R. Bond, E. Calabrese, D. Crichton, M. J. Devlin, S. Dicker, et al., JCAP **4**, 014 (2014), 1301.1037.
[27] S. M. Simon, J. W. Appel, L. E. Campusano, S. K. Choi, K. T. Crowley, T. Essinger-Hileman, P. Gallardo, S. P. Ho, A. Kusaka, F. Nati, et al., Journal of Low Temperature Physics **184**, 534 (2016), 1511.04760.
[28] R. A. Sunyaev and I. B. Zeldovich, ARA&A **18**, 537 (1980).
[29] D. Alonso, T. Louis, P. Bull, and P. G. Ferreira, Phys. Rev. **D94**, 043522 (2016), 1604.01382.
[30] LSST Collaboration, P. A. Abell, J. Allison, S. F. Anderson, J. R. Andrew, J. R. P. Angel, L. Armus, D. Arnett, S. J. Asztalos, T. S. Axelrod, et al., arXiv e-prints (2009), 0912.0201.
[31] R. S. de Jong, S. Barden, O. Bellido-Tirado, J. Brynnel, C. Chiappini, É. Depagne, R. Haynes, D. Johl, D. P. Phillips, O. Schnurr, et al., in *Ground-based and Airborne Instrumentation for Astronomy V* (2014), vol. 9147 of *Proc. SPIE*, p. 91470M.
[32] M. Shimon, S. Sadeh, and Y. Rephaeli, MNRAS **412**, 1895 (2011), 1009.4110.
[33] W. Hu and A. V. Kravtsov, Astrophys. J. **584**, 702 (2003), astro-ph/0203169.
[34] D. Alonso, P. Bull, P. G. Ferreira, R. Maartens, and M. G. Santos, Astrophys. J. **814**, 145 (2015), 1505.07596.
[35] Planck Collaboration, P. A. R. Ade, N. Aghanim, M. I. R. Alves, C. Armitage-Caplan, M. Arnaud, M. Ashdown, F. Atrio-Barandela, J. Aumont, H. Aussel, et al., A&A **571**, A1 (2014), 1303.5062.
[36] D. Blas, J. Lesgourgues, and T. Tram, JCAP **7**, 034 (2011), 1104.2933.
[37] A. Benoit-Lévy, K. M. Smith, and W. Hu, Phys. Rev. D **86**, 123008 (2012), 1205.0474.
[38] J. Liu, J. C. Hill, B. D. Sherwin, A. Petri, V. Böhm, and Z. Haiman, ArXiv e-prints (2016), 1608.03169.
[39] M. Lima and W. Hu, Phys. Rev. D **70**, 043504 (2004), astro-ph/0401559.
[40] R. E. Smith and L. Marian, MNRAS **418**, 729 (2011), 1106.1665.
[41] E. Krause and T. Eifler, ArXiv e-prints (2016), 1601.05779.
[42] M. Costanzi, F. Villaescusa-Navarro, M. Viel, J.-Q. Xia, S. Borgani, E. Castorina, and E. Sefusatti, JCAP **12**, 012 (2013), 1311.1514.
[43] W. Cui, S. Borgani, K. Dolag, G. Murante, and L. Tornatore, MNRAS **423**, 2279 (2012), 1111.3066.
[44] https://github.com/dhanson/quicklens